Mechanisms of Exchange Modulation in Trimethylenemethane-type Biradicals: The Roles of Conformation and Spin Density

David A. Shultz,*,† Rosario M. Fico, Jr.,† Hyoyoung Lee,†,|| Jeff W. Kampf,‡ Kristin Kirschbaum,§ A. Alan Pinkerton,§ and Paul D. Boyle†

Contribution from the Department of Chemistry, North Carolina State University, Raleigh, North Carolina 27695-8204, Department of Chemistry, University of Michigan, Ann Arbor, Michigan 48109-1055, and Department of Chemistry, University of Toledo, Toledo, Ohio 43606

Received August 6, 2003; E-mail: david_shultz@ncsu.edu

Abstract: The molecular structures and magnetic properties of six dinitroxide biradicals are described. Five of the dinitroxides are trimethylenemethane-type (TMM-type) biradicals; that is, the intramolecular exchange parameter, J, is modulated by a carbon–carbon double bond. However, the efficacy of the carbon–carbon double bond as an exchange coupler is determined by the molecular conformation. Our results show that the exchange parameters correlate with phenyl-ring torsion angles (ϕ) via a simple Karplus–Conroy-type relation: $J = 44 \cos^2 \phi - 17$. Comparison of these results to those obtained for our isostructural series of bis(semiquinone) biradicals shows that both the magnitude of J and the resistance of ferromagnetic J to bond torsions is proportional to the spin density adjacent to the exchange coupler.

Introduction

Large amplitude bond torsions can dramatically affect exchange couplings in organic biradicals when the bonds connect spin-containing groups to exchange-coupling fragments.[1] Several examples of this structure–property relationship have been noted for *meta*-phenylene-type biradicals (Figure 1).[2–9] Trimethylenemethane-type (TMM-type) biradicals, Figure 1, having the 1,1-diarylethene moiety are an interesting class of molecules with which to study this phenomenon because diarylethene conformation and dynamics have been elucidated[10] and, as discussed below, the conformation can be "controlled"
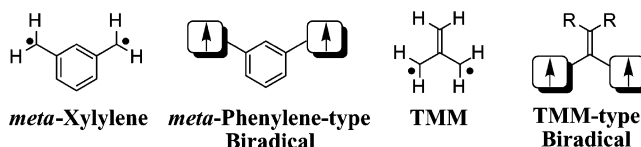
† North Carolina State University.
‡ University of Michigan.
§ University of Toledo.
|| Current address: Organic Materials Device Team, Telecommunication Basic Research, Electronics and Telecommunications Research Institute (ETRI), 161 Kajong-dong, Yusong-Gu, Taejon, 305-350, Korea.

(1) Shultz, D. A. Conformational Exchange Modulation in Trimethylenemethane (TMM)-Type Biradicals. In *Magnetic Properties of Organic Materials*; Lahti, P., Ed.; Marcel Dekker: New York, 1999.
(2) Dei, A.; Gatteschi, D.; Sangregorio, C.; Sorace, L.; Vaz, M. G. F. *Inorg. Chem.* **2003**, *42*, 1701–1706.
(3) Fujita, J.; Tanaka, M.; Suemune, H.; Koga, N.; Matsuda, K.; Iwamura, H. *J. Am. Chem. Soc.* **1996**, *118*, 9347–9351.
(4) Okada, K.; Imakura, T.; Oda, M.; Murai, H.; Baumgarten, M. *J. Am. Chem. Soc.* **1996**, *118*, 3047–3048.
(5) Adam, W.; van Barneveld, C.; Bottle, S. E.; Engert, H.; Hanson, G. R.; Harrer, H. M.; Heim, C.; Nau, W. M.; Wang, D. *J. Am. Chem. Soc.* **1996**, *118*, 3974–3975.
(6) Fang, S.; Lee, M.-S.; Hrovat, D. A.; Borden, W. T. *J. Am. Chem. Soc.* **1995**, *117*, 6727–6731.
(7) Silverman, S. K.; Dougherty, D. A. *J. Phys. Chem.* **1993**, *97*, 13273–13283.
(8) Kanno, F.; Inoue, K.; Koga, N.; Iwamura, H. *J. Am. Chem. Soc.* **1993**, *115*, 847–850.
(9) Dvolaitzky, M.; Chiarelli, R.; Rassat, A. *Angew. Chem., Int. Ed. Engl.* **1992**, *31*, 180–181.
(10) Kaftory, M.; Nugiel, D. A.; Biali, S. E.; Rappoport, Z. *J. Am. Chem. Soc.* **1989**, *111*, 8181–8191.

Figure 1. Biradical classifications.

meta-Xylylene   *meta*-Phenylene-type Biradical   TMM   TMM-type Biradical

in a comparatively straightforward way. Along these lines, we recently reported that conformation controls both ferromagnetic and antiferromagnetic exchange contributions to J via a simple torsional model given by eq 1 (ϕ is the average torsion angle between semiquinone rings and the ethene coupler), using the series of bis(semiquinone) biradicals shown in Figure 2.[11]

$$J = A \cos^2 \phi + B \qquad (1)$$

Equation 1 contains a $\cos^2 \phi$ term because overlap of 2p-π orbitals of the semiquinone groups with those of the ethene coupler varies as the cosine-squared of the torsion angles (ϕ) between the two groups.[12] Because of the small number of data points, and for comparative purposes, our primary concern is to keep eq 1 simple. To achieve this, we consider only a single trigonometric function and we use an average of the two torsion angles.

We showed that J for $1(SQZnL)_2$, $3(SQZnL)_2$, $4(SQZnL)_2$, and $6(SQZnL)_2$ varies according to eq 1, where $A = +213$ cm^{-1} and $B = -44$ cm^{-1}.[11] These parameters give net ferromagnetic

(11) Shultz, D. A.; Fico, R. M., Jr.; Bodnar, S. H.; Kumar, R. K.; Vostrikova, K. E.; Kampf, J. W.; Boyle, P. D. *J. Am. Chem. Soc.* **2003**, *125*, 11761–11771.
(12) Streitwieser, A., Jr. *Molecular Orbital Theory for Organic Chemists*; Wiley & Sons: New York, 1961.
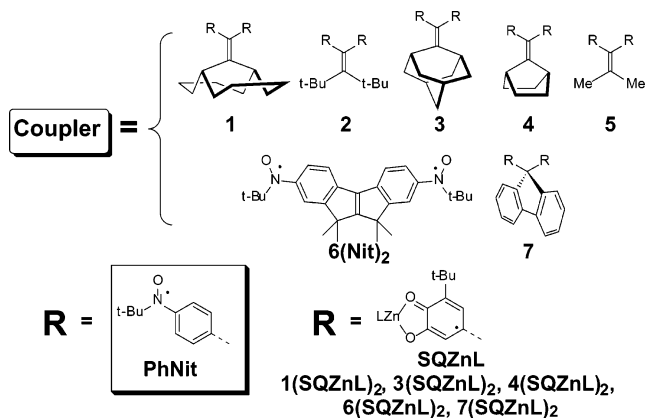
Figure 2. TMM-type dinitroxide and bis(semiquinone) biradicals.

coupling over a wide range of semiquinone ring torsion angles, ϕ. At severe torsion angles ($\phi >$ ca. 60°), the net antiferromagnetic exchange is caused by a molecular conformation in which the semiquinone rings are "stacked". This stacking is equivalent to Anderson's incipient bonding[13,14] and provides an effective antiferromagnetic pathway.

Herein, we present molecular structures for a related series of dinitroxide biradicals, **1(PhNit)₂**−**4(PhNit)₂**, **6(Nit)₂**, and **7-(PhNit)₂**. The exchange parameters for this series also show $\cos^2 \phi$ dependence (ϕ = average phenyl ring torsion angle) despite the added C−N bond torsions of the nitroxide groups. Most importantly, the new parameters *A* and *B* in eq 1 reflect spin density differences between semiquinone and phenyl-nitroxide radical fragments.

Results and Discussion

Biradical Design Elements. The generalized TMM-type biradicals have lower symmetry (C_2 or C_{2v}) than the parent trimethylenemethane, TMM (D_{3h}). For biradicals of lower symmetry, the energetic preference for the high-spin state should decrease.[11] In addition, when the spin-containing groups contain heteroatoms at active positions (positions having positive spin densities), the energy gap between the SOMOs widens further according to the heteroatom electronegativities. Despite this symmetry lowering and SOMO energy difference, the triplet-state of heteroatom-substituted TMM-type biradicals is still predicted to be the ground state.[15−19]

Design elements of generalized TMM-type biradicals were discussed previously[11,20] and are summarized in Figure 3. These biradicals are optimal for studying conformational *J*-modulation, because of the proximity of the capping groups to the spin-containing groups. The steric interaction between these two fragments that results from this close proximity is a function of the composition of the capping group. The resulting torsions of the spin-containing π-systems relative to the ethene coupler
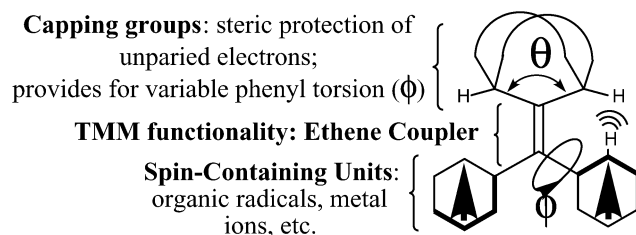
(13) Anderson, P. W. *Phys. Rev.* **1959**, *115*, 2−13.
(14) Hatfield, W. E. Properties of Condensed Compounds (Compounds with Spin Exchange). In *Theory and Applications of Molecular Paramagnetism*; Boudreaux, E. A., Mulay, L. N., Eds.; Wiley-Interscience: New York, 1976; Chapter 7, pp 381−385.
(15) Borden, W. T.; Davidson, E. R. *J. Am. Chem. Soc.* **1977**, *99*, 4587−4594.
(16) Borden, W. T. *Diradicals*; Wiley: New York, 1982.
(17) Dougherty, D. A. *Acc. Chem. Res.* **1991**, *24*, 88−94.
(18) Rajca, A. *Chem. Rev.* **1994**, *94*, 871−893.
(19) Borden, W. T.; Iwamura, H.; Berson, J. A. *Acc. Chem. Res.* **1994**, *27*, 109−116.
(20) Shultz, D. A.; Boal, A. K.; Lee, H.; Farmer, G. T. *J. Org. Chem.* **1999**, *64*, 4386−4396.

Capping groups: steric protection of unpaired electrons; provides for variable phenyl torsion (ϕ)

TMM functionality: Ethene Coupler

Spin-Containing Units: organic radicals, metal ions, etc.

Figure 3. Generalized TMM-type biradical design elements.

1(PhNit)₂　　**2(PhNit)₂**

3(PhNit)₂　　**4(PhNit)₂**
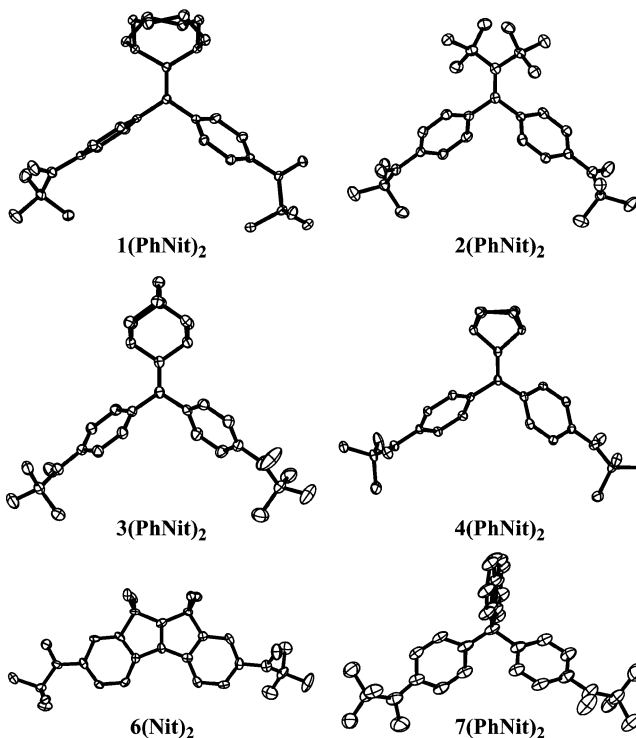
6(Nit)₂　　**7(PhNit)₂**

Figure 4. Thermal ellipsoid plots for **1(PhNit)₂**−**4(PhNit)₂**, **6(Nit)₂**, and **7(PhNit)₂**. Hydrogens are omitted for clarity.

cause steric inhibition of resonance delocalization that attenuates the effectiveness of the coupler to high-spin couple unpaired electrons.[1,11,19]

To further elucidate this fundamental structure−property relationship, the TMM-type dinitroxides in this study are designed to have a range of aryl torsion angles that were determined by X-ray crystallography and are presented in the next section.

Molecular Structures. The syntheses and EPR spectra of **1(PhNit)₂**−**4(PhNit)₂**, **6(Nit)₂**, and **7(PhNit)₂** were presented earlier.[20] Iwamura reported the magnetic properties of **5-(PhNit)₂**,[21,22] but in our hands this biradical was sufficiently unstable so as to prevent formation of X-ray-quality crystals. Thermal ellipsoid plots for **1(PhNit)₂**−**4(PhNit)₂**, **6(Nit)₂**, and **7(PhNit)₂** are shown in Figure 4. Important torsion angles are listed in Table 1, and a complete record of bond lengths and angles can be found in the Supporting Information.

As predicted,[20] the phenyl ring torsions decrease in going from **1(PhNit)₂** to **6(Nit)₂**. By contrast, the nitroxide N−O bond torsions vary randomly with a series average N−O torsion of

(21) Matsumoto, T.; Ishida, T.; Koga, N.; Iwamura, H. *J. Am. Chem. Soc.* **1992**, *114*, 9952−9959.
(22) Matsumoto, T.; Koga, N.; Iwamura, H. *J. Am. Chem. Soc.* **1992**, *114*, 5448−5449.

Table 1. Phenyl Ring and Nitroxide Group Torsion Angles in Dinitroxides **1(PhNit)₂**−**4(PhNit)₂**, **6(Nit)₂**, and **7(PhNit)₂**[a]

biradical	phenyl torsions[a]	average phenyl torsion	nitroxide torsions[b]	average nitroxide torsion
1(PhNit)₂	65.92 ± 0.05	74.2 ± 8.2	40.68 ± 0.1	31.9 ± 8.7
	82.37 ± 0.05		23.14 ± 0.1	
2(PhNit)₂	54.3 ± 0.1	54.9 ± 0.6	9.8 ± 0.2	10.5 ± 0.7
	55.5 ± 0.1		11.1 ± 0.2	
3(PhNit)₂	54.73 ± 0.08	54.1 ± 0.6	11.23 ± 0.07	10.6 ± 0.7
	53.47 ± 0.08		9.9 ± 0.1	
	at 25 K: 50.7 ± 0.4	52.5 ± 1.8	at 25 K: 36.8 ± 1.1	28.5 ± 8.3
	54.3 ± 0.4		20.2 ± 1.0	
4(PhNit)₂	43.19 ± 0.11	47.0 ± 3.8	31.4 ± 0.2	31.4 ± 0.2
	50.84 ± 0.11		31.3 ± 0.2	
6(PhNit)₂	1.9 ± 0.3	1.9 ± 0.3	30.1 ± 0.2	29.3 ± 0.9
	1.8 ± 0.3		28.4 ± 0.2	
7(PhNit)₂[c]	39.2 ± 0.5	40.1 ± 0.9	13.5 ± 0.4	18.9 ± 5.4
	41.0 ± 0.5		24.3 ± 0.5	

[a] Phenyl torsion angle defined as the angle between the plane of a phenyl ring and the plane containing the ethene coupler. [b] Nitroxide torsion angle defined as $O-N-C_{phenyl}-C_{phenyl}$. [c] **7(PhNit)₂** torsion angles defined as bond torsion between the phenyl rings through the sp^3 carbon of the fluorenyl group.

24.5 ± 12.8°. The phenyl ring torsions for the dinitroxides **1-(PhNit)₂**, **4(PhNit)₂**, and **6(Nit)₂** parallel the semiquinone ring torsions for the corresponding bis(semiquinone)s **1(SQZnL)₂**, **4(SQZnL)₂**, and **6(SQZnL)₂**, again demonstrating the role of the capping group in controlling the conformation of these TMM-type biradicals. Finally, **2(PhNit)₂** has no bis(semiquinone) analogue. This dinitroxide is interesting because of the noteworthy torsion of the ethene C=C, 27.5 ± 0.6° − a value quite similar to 24° for 1,1-diphenyl-2,2-di-*tert*-butylethene.[23]

Structural Phase Transition in Crystals of 3(PhNit)₂. We recently reported magnetic hysteresis in crystals of **3(PhNit)₂**.[24] This is the only dinitroxide biradical that we have studied that exhibits this phenomenon. We also note that the bis(phenoxy) and bis(semiquinone) biradical analogues exist as multiple rotamers in frozen solution.[11,25] Again, other related biradicals do not show this behavior. We feel that there is now ample experimental evidence that the adamantyl capping group results in shallow conformational potential energy surface for 1,1-diarylethenes that can accommodate several metastable conformations, at least in frozen solution.

The molecular structure of **3(PhNit)₂** below and above the phase transition as well as pictures of the unit cell below and above the transition are shown in Figure 5. Torsion angles for both the 25 and the 158 K structures are listed in Table 1.

As seen in Figure 5A, the molecular structures of **3(PhNit)₂** at 158 and 25 K differ significantly. The differences in molecular structures can be explained by three primary displacive components. The first two components are nitroxide and *tert*-butyl torsions, and these differences are summarized in Table 2. The largest numeric change (Δtorsion = −57.9°) is the torsion of the *tert*-butyl group relative to the nitroxide group. This brings the *tert*-butyl group from an eclipsed conformation to gauche relative to the nitroxide group and presumably lowers the steric repulsion between the methyl groups and the oxygen atom, O2. The second largest change (Δtorsion = 24°) is the torsion of the nitroxide group around the N−C_phenyl bond. At 25 K, greater nitroxide torsion is observed.

The third component of displacement involves the C12 phenyl ring. The dihedral angle between the phenyl group at 25 K and

the same phenyl group at 158 K is 11.1°. Although the angular displacement seems modest, it results in large linear displacements on the periphery of the molecule. The displacement due to this "dihedral deformation" is 0.65 Å at C15 and would give even more pronounced displacements for atoms in the *tert*-butylnitroxide group. Taken together, the two torsions and the dihedral deformation result in overall atomic displacements for C18, N2, and O2 of 0.93, 1.12, and 1.78 Å, respectively. It is the sum of these changes which brings the intermolecular nitroxide−nitroxide distance from ~5.4 to ~2.5 Å. In contrast, the corresponding atomic displacements for the other nitroxide group C5, N1, O1, and C1 are 0.12, 0.15, 0.26, and 0.14 Å, respectively.

Another point worth noting in Figure 5A is that the probability displacement ellipsoids of the *tert*-butylnitroxide group (N2−O2) involved in the quasi-dimerization suggest significantly higher amplitudes of internal motion at 158 K than does the other nitroxide group (N1−O1). This observation is chemically significant because it indicates that at nearly 90 K above the transition temperature the dynamic aspects of the crystal structure are already giving an indication of a possible pathway to the low-temperature structure. To put this observation on a more quantitative basis, the anisotropic displacement parameters (ADPs) were subjected to a **TLS** rigid-body[26] motion analysis[27,28] as well as a segmented-body motion analysis using the Dunitz−White model for internal torsions.[29] The residual[30] for the rigid-body motion analysis was 0.36, indicating that the molecular motion in the crystal cannot be adequately described as a rigid body. A number of internal torsional (librational) axes were added to improve the fit. The best model included six internal librational axes and yielded a residual of 0.13. The internal libration axes were defined as follows: ϕ_1, C5···C1 vector; ϕ_2, N1−C1 vector; ϕ_3, C8···C5 vector; ϕ_4, C15···C18 vector; ϕ_5, N2−C18; ϕ_6, C12···C15 vector. The mean square displacement amplitudes for these axes are given in degrees

(23) Mugnoli, A.; Simonetta, M. *J. Chem. Soc., Perkin Trans. 2* **1976**, 1831−1835.
(24) Shultz, D. A.; Fico, R. M., Jr.; Boyle, P. D.; Kampf, J. W. *J. Am. Chem. Soc.* **2001**, *123*, 10403−10404.
(25) Shultz, D. A.; Boal, A. K.; Farmer, G. T. *J. Am. Chem. Soc.* **1997**, *119*, 3846−3847.
(26) The term **TLS** derives from names of the tensors from a rigid body motion analysis of the individual atomic ADPs. The **T** refers to the translational tensor, the **L** refers to the librational tensor, and the **S** refers to the screw tensor, which represents the correlation between the translational and librational motions.
(27) Schomaker, V.; Trueblood, K. N. *Acta Crystallogr.* **1968**, *B24*, 63−76.
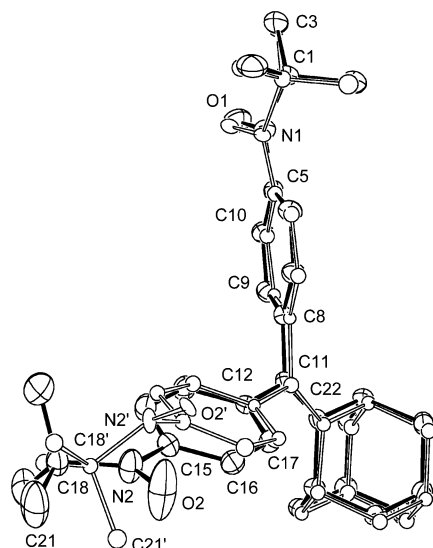(28) Dunitz, J. D.; Schomaker, V.; Trueblood, K. N. *J. Phys. Chem.* **1988**, *92*, 856−867.
(29) Dunitz, J. D.; White, D. N. J. *Acta Crystallogr.* **1973**, *A29*, 93−94.
(30) Residual is defined as: $R_{wU} = [\sum w^{ij}(\Delta U^{ij})^2 / \sum w^{ij}(U_{obs}^{ij})^2]^{1/2}$.

A

B

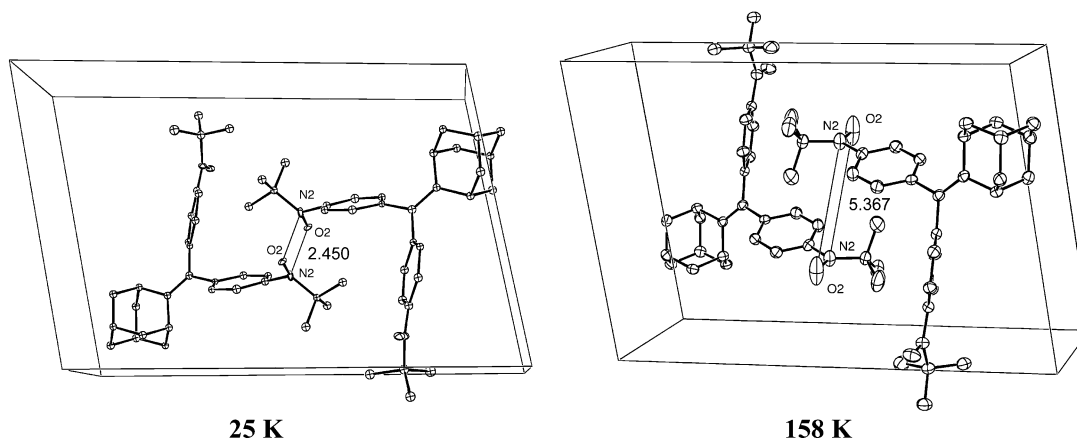**25 K**   **158 K**

Figure 5. (A) Overlay of thermal ellipsoid plots for **3(PhNit)₂** below (25 K; open ellipsoids) and above (158 K; hatched ellipsoids) the structural phase transition. (B) Unit cell comparison. Intermolecular N···O contacts are 2.450 Å at 25 K (left) and 5.367 Å at 158 K (right).

Table 2. Structural Differences for **3(PhNit)₂** above and below the Phase Transition

bond torsion	25 K (deg)	158 K (deg)	Δtorsion (25–158 K; deg)
C22−C11−C12−C17	56.3	54.8	1.5
O2−N2−C15−C16	36.7	12.7	24.0
O2−N2−C18−C21	−73.1	−15.2	−57.9
C22−C11−C8−C9	55.5	56.2	−0.7
O1−N1−C5−C10	20.3	13.2	7.1
O1−N1−C1−C3	−20.7	−7.3	−13.4

squared, $\langle\phi_1^2\rangle$, 20(4); $\langle\phi_2^2\rangle$, 19(4); $\langle\phi_3^2\rangle$, 9(5); $\langle\phi_4^2\rangle$, 125(4); $\langle\phi_5^2\rangle$, 87(4); $\langle\phi_6^2\rangle$, 19(5). While the librations for both of the phenyl groups are not significantly different, the librations of the respective nitroxide and *tert*-butyl groups are significantly larger for the groups (N2−O2, and C19, C20, C21) which undergo the twisting in the low-temperature phase. An alternative six internal axis model put libration axes for ϕ_1 and ϕ_4 along the C−N bond vectors, N1−C5 and N2−C15, respectively, with only the corresponding oxygens, O1 and O2, as the atoms affected by these internal librations. In this case, the fit was slightly worse with a residual of 0.14, and mean square displacement amplitudes of 55(12) and 344(12) deg², respectively.

These structural changes appear to be driven by temperature-dependent changes in the potential energy surface of the crystal lattice rather than due to the shape of the potential energy surface of isolated 1,1-diarylmethyleneadamantanes that we originally proposed.[24] Nevertheless, N2−O2 torsion makes an important contribution in bringing nitroxide groups of two different biradicals into close proximity, creating a diamagnetic dimer. The spins of the remaining N1−O1 nitroxide groups are by comparison uncoupled, thereby explaining the observed magnetic behavior.[24]

Solid-State Magnetic Susceptibility Measurements. Plots of the magnetic susceptibility data for all of the compounds (as films in poly[vinyl chloride], see below) are plotted in Figure 6.[31] Modeling the temperature-dependent χT products of biradicals having monoradical impurity can be achieved by fitting to a field-independent van Vleck expression, eq 2,[32,33]

$$\chi T = (x)\frac{2Ng^2\beta^2}{k[3 + e^{-2J/kT}]} + (1 - x)\frac{Ng^2\beta^2}{2k} \qquad (2)$$

where *x* is the mole fraction of biradical, *g* is the isotropic Landé

(31) See Supporting Information for all magnetic susceptibility plots and fits.
(32) Kahn, O. *Molecular Magnetism*; VCH: New York, 1993.
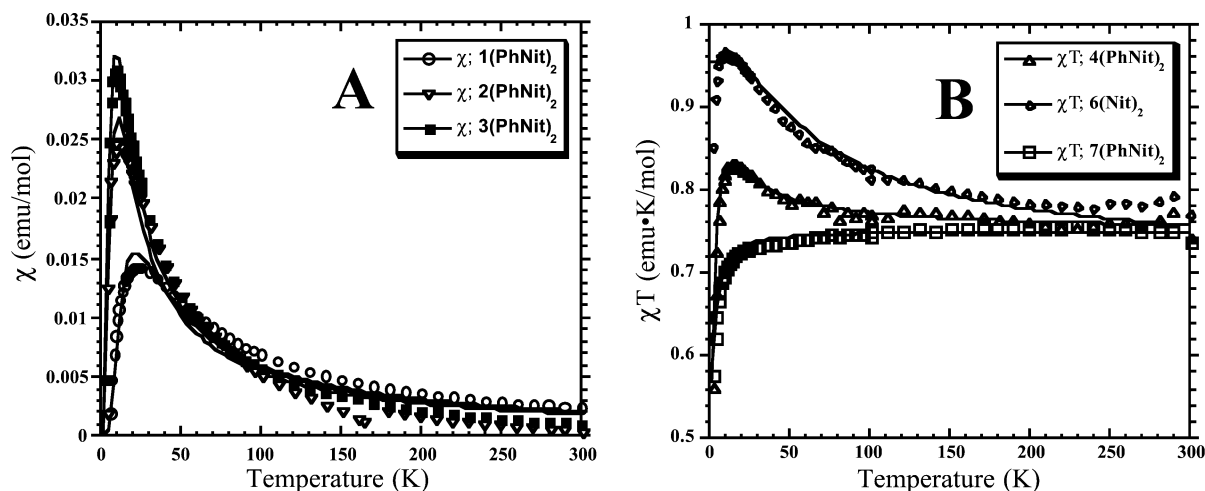(33) Bleaney, B.; Bowers, K. D. *Proc. R. Soc. London* **1952**, *A214*, 451−465.

Figure 6. (A) χ versus *T* plots: **1(PhNit)₂** (○); **2(PhNit)₂** (▽); **3(PhNit)₂** (■). (B) χ*T* versus *T* plots: **4(PhNit)₂** (△); **6(Nit)₂** (◇); **7(PhNit)₂** (□) as films in poly[vinyl chloride] (see text for details).

constant (g = 2.0023), β is the Bohr magneton, T is temperature in Kelvin, k is Boltzmann's constant, and J is the intramolecular nitroxide−nitroxide exchange coupling parameter. When J < 0, χ exhibits a maximum at $T_{max} = 1.285J/k$.[32] Therefore, in singlet ground-state biradicals, χ versus T plots are preferred over χT versus T plots, while the opposite is true for triplet ground-state biradicals.[32] The singlet- and triplet-state energies were derived using the Hamiltonian, $H = -2J\hat{S}_1\cdot\hat{S}_2$, where $\hat{S}_1$ and $\hat{S}_2$ are the spin operators for the nitroxides. The decrease (increase) in the χT (χ) data at low temperatures was accounted for with a Weiss mean-field correction, using the expression $\chi_{eff} = \chi/(1 - \vartheta\chi)$, where $\vartheta = 2zJ'/(Ng^2\beta^2)$.[34] The origin of zJ' may be zero-field splitting, intermolecular interaction, saturation effects, or some combination of all three.[35] The other terms have their usual meanings.[34] All curve fit results are presented in Table 3.

The fit parameters for a crystalline sample of **4(PhNit)₂** show that zJ' is within 1 order of magnitude of the exchange parameter J.[36] As such, the mean-field correction is inappropriate,[34] and therefore the magnetic susceptibility for all biradicals was measured on solid solutions of the biradicals in poly[vinyl chloride] in an attempt to attenuate intermolecular exchange interactions. Measuring the temperature-dependent magnetic susceptibility in polymer films also affords us the opportunity to determine an exchange parameter for **3(PhNit)₂** that undergoes a hysteretic phase transition in the crystal form (see above). Perusal of Table 3 shows that, for most of the compounds, nearly identical J-values are estimated from crystal and PVC film samples, suggesting similar molecular conformations in crystal and PVC films. Because we obtained reasonable results for all compounds as solutions in PVC, these results are displayed in Figure 6.

The exchange coupling for **1(PhNit)₂** is antiferromagnetic ($J \approx -12$ cm⁻¹) and compares reasonably with the value

(34) O'Connor, C. J. *Prog. Inorg. Chem.* **1982**, *29*, 203−283.
(35) Caneschi, A.; Dei, A.; Mussari, C. P.; Shultz, D. A.; Sorace, L.; Vostrikova, K. E. *Inorg. Chem.* **2002**, *41*, 1086−1092.
(36) There is no pattern to the variation in the zJ' term within our series of biradicals. Although we have no explanation, our observation is consistent with the lack of a pattern noted by Veciana et al.: Veciana, J.; Cirujeda, J.; Novoa, J. J.; Deumal, M. Supramolecular Architectures and Magnetic Interactions in Crystalline α-Nitronyl Nitroxide Radicals. In *Magnetic Properties of Organic Materials*; Lahti, P. M., Ed.; Marcel Dekker: New York, 1999; pp 573−600.
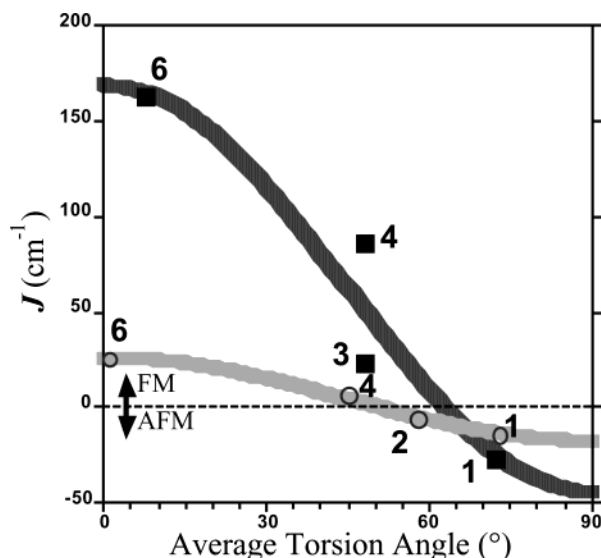
Table 3. Magnetic Data for Dinitroxides **1(PhNit)₂−7(PhNit)₂**[a]

biradical	purity[b]	sample form	zJ' (cm⁻¹)	J (cm⁻¹)	ref
1(PhNit)₂	96%	crystal	+0.25	−14.03 ± 0.12[a]	this work
	86%	PVC film	e	−11.8 ± 1.2[c]	
2(PhNit)₂		crystal	e	see text	this work
	74%	PVC film	e	−5.75 ± 0.31[c]	
3(PhNit)₂		crystal		hysteresis	this work
	79%	PVC film	e	−5.11 ± 0.24[c]	
4(PhNit)₂	100%	crystal	−3.0	+6.79 ± 0.18[c]	this work
	100%	PVC film	−0.79	+6.07 ± 0.15[c]	
5(PhNit)₂	88%	crystal	−3.82[d]	+5.24	22
		PVC film	e		
6(Nit)₂	80%	crystal	−2.14	+25.5 ± 1.6[a]	this work
	95%	PVC film	e	+26.35 ± 1.73[c]	
7(PhNit)₂	55%	crystal	−0.56	−2.61 ± 0.01[c]	this work
	24%	PVC film	e	−2.85 ± 0.13[c]	

[a] Magnetic susceptibility measured by SQUID magnetometry between 2 and 300 K with an applied field of 0.5 T. [b] The term "purity" refers to the percent biradical in the sample, the remainder being monoradical. The biradical purities were determined by iterative fitting of the magnetic susceptibility data. [c] Magnetic susceptibility measured by SQUID magnetometry between 300 and 2 K with an applied field of 1 T. [d] This is the reported Weiss constant, θ, converted to cm⁻¹. [e] Data were fit without a Weiss mean-field correction term, zJ'.

calculated from the EPR Curie plot (−24 cm⁻¹).[20] The net antiferromagnetic coupling is due to the molecular conformation: the large bond torsions compromise the coupler's ability to effect ferromagnetic coupling.

We were unable to obtain reasonable fits to the magnetic susceptibility data for crystals of **2(PhNit)₂** using either eq 2 or an alternating 1-D chain model.[37,38] Therefore, the magnetic susceptibility data in a PVC film were used for subsequent analysis. We attribute the linear Curie plot we reported for a frozen 2-methyltetrahydrofuran solution of **2(PhNit)₂**[20] to an overall weaker J in frozen solution as compared to both the solid and the PVC film.

As discussed above, crystals of **3(PhNit)₂** undergo a structural phase transition, so only a film was useful for estimating J.

(37) Hatfield, W. E.; Helms, J. H. *Mater. Sci.* **1991**, *17*, 21−31.
(38) Georges, R.; Borras-Almenar, J. J.; Coronado, E.; Curely, J.; Drillon, M. One-dimensional Magnetism: An Overview of the Models. In *Magnetism: Molecules to Materials, Models and Experiments*; Miller, J. S., Drillon, M., Eds.; Wiley-VCH: New York, 2001; pp 1−47.

Figure 7. "Karplus−Conroy-type" relationship for electron spin exchange coupling in bis(semiquinone) biradicals **1(SQZnL)₂**, **3(SQZnL)₂**, **4-(SQZnL)₂**, and **6(SQZnL)₂** (■; dark curve), and dinitroxides **1(PhNit)₂**−**4(PhNit)₂** and **6(Nit)₂** (○; light curve). For clarity, data points are marked by the coupler (see Figure 2) and not the molecule designations. Datum for **2(PhNit)₂** is from PVC film.

Like **1(PhNit)₂** and **2(PhNit)₂**, the exchange parameter is antiferromagnetic.

Dinitroxide **4(PhNit)₂** is the first biradical in the series to exhibit ferromagnetic intramolecular exchange coupling. J-values for the crystal and PVC film are comparable ($J \approx +6.4 \pm 0.3$ cm^{-1}) and slightly more ferromagnetic than the value for **5(PhNit)₂** reported by Iwamura.[21,22]

The strongest net ferromagnetic coupling in the series is for **6(Nit)₂** in which the coupler is part of an essentially planar π-system. The weakest net intramolecular exchange coupling is for **7(PhNit)₂** that lacks a C=C coupler. This again shows that an ethene coupler is a more effective exchange coupler than an sp^3 carbon.[11]

The exchange coupling parameters for those dinitroxides having a simple C=C coupler (**1(PhNit)₂**−**4(PhNit)₂**, **6(Nit)₂**) can be correlated to the average phenyl ring torsion angles (ϕ) via a Karplus−Conroy-type relation,[39] eq 1.[40] The data are displayed in Figure 7, along with the corresponding data for bis(semiquinone)s. The J-values used for Figure 7 are those calculated for crystalline samples, except for that of **2(PhNit)₂** with comes from our fit of the film data. For three of the four dinitroxides, this ensures that the J-values correspond to the same conformations measured by X-ray crystallography, but necessarily omits data for **3(PhNit)₂**. For the dinitroxides, the "fit" to eq 1 gives $A = +44$ cm^{-1} and $B = -17$ cm^{-1}. Our omission of nitroxide torsions is validated by the acceptable correlation of J with average phenyl torsion displayed in Figure 7.[41] Given the simplicity of our model (eq 1), the A- and B-terms should be considered semiquantitative, as suggested by the

thickness of the curves in Figure 7.[42] Nevertheless, we stated previously that the A-term should be a function of both the coupler and the spin density in the spin-containing group and that the B-term should be proportional to the through-space antiferromagnetic interaction. The ratio of the bis(semiquinone) to dinitroxide A-terms from eq 1 is $213/44 \approx 5$. This ratio is nearly equal to the ratio of the corresponding semiquinone ring to phenyl-nitroxide ring spin densities: $\rho_{SQ}/\rho_{PhNit} \approx 0.5/0.125 = 4$.[43−45] Thus, the phenyl-*tert*-butyl-nitroxide group presents less spin density to the coupler (which is measured by the magnitude of A) than does the semiquinone group. Considering the overall weaker coupling of the dinitroxides, the A-term in eq 1 is smaller, and so is the antiferromagnetic B-term as compared to the bis(semiquinone)s. This spin-density relationship with J is suggested by eq 3:

$$J = J_0\rho_i \cdot \rho_j \qquad (3)$$

where ρ_i and ρ_j are the spin densities on the atoms that are attached to the coupler, and J_0 is the intrinsic exchange parameter for the parent biradical in which $\rho_i = \rho_j = 1$.[18,46−48] Thus, the A-term in eq 1 tracks the conformation-dependent change in spin density "available" to the coupler to affect ferromagnetic exchange.[49]

As noted previously, TMM-type bis(semiquinone) biradicals exhibit net ferromagnetic exchange coupling over a broad range of semiquinone ring torsions ($\leq \sim 60°$).[11] By comparison, TMM-type dinitroxides exhibit net ferromagnetic coupling over a smaller range of phenyl ring torsions ($\leq \sim 50°$). This can be seen by comparing the torsion angles for which the curves calculated by eq 1 cross the horizontal dashed line at $J = 0$ in Figure 7. Thus, the intrinsically weaker exchange coupling in the dinitroxides is more sensitive to bond torsions as compared to the bis(semiquinone)s. It is important to note that the dinitroxides presented here also have a range of nitroxide torsion angles with respect to the phenyl ring; nevertheless, our simple approach that takes into account only phenyl ring torsion is effective at communicating the conformational exchange modulation.

Conclusions

We have shown a torsional dependence of electron spin−spin exchange coupling in TMM-type dinitroxide biradicals, and we compared this torsional dependence to an analogous series of TMM-type bis(semiquinone) biradicals. Our findings can be summarized by comparing the following relations.

TMM-type dinitroxides:

$$J_{Nit−Nit} \, (\text{cm}^{-1}) = 44 \cos^2\phi - 17$$

TMM-type bis(semiquinone)s:

$$J_{SQ−SQ} \, (\text{cm}^{-1}) = 213 \cos^2\phi - 44$$

In agreement with theory,[18,46,47] the weaker ferro- (A-term) and antiferromagnetic (B-term) exchange contributions of the

(39) Karplus, M. *J. Am. Chem. Soc.* **1963**, *85*, 2870−2871.
(40) Interestingly, for the four compounds for which we have both crystal and PVC magnetic susceptibility data sets, the plot of J(PVC) vs J(crystal) is linear with a slope of unity. Thus, the same angular correlation (i.e., the same A- and B-terms) exists both in solution and in the solid state. In addition, the film data for **3(PhNit)₂** give a J-value that falls directly on the line in Figure 7 using the "undimerized" crystallographic torsion angles.
(41) As shown in Table 1, the average nitroxide torsions range from 10° to 30°. This portion of a cos^2 curve has relatively little slope, so changes in J for this range of torsion are expected to be minimal.

(42) The fit routine gives $A = 44 \pm 3$ and $B = -17 \pm 2$.
(43) Aurich, H. G.; Hahn, K.; Stork, K.; Weiss, W. *Tetrahedron* **1977**, *33*, 969−975.
(44) Shultz, D. A.; Gwaltney, K. P.; Lee, H. *J. Org. Chem.* **1998**, *63*, 769−774.
(45) Wheeler, D. E.; Rodriquez, J. H.; McCusker, J. K. *J. Phys. Chem. A* **1999**, *103*, 4101−4112.

dinitroxides can be traced to the smaller spin densities at the point of attachment to the ethene coupler.

Experimental Section

Magnetometry. Magnetic susceptibilities were measured on a Quantum Design MPMS-XL7 SQUID magnetometer using an applied field of 0.5 or 1 T for Curie plots. Data for crystalline samples were corrected for molecular diamagnetism using Pascal's constants, while PVC film data were corrected for both diamagnetism and paramagnetic impurities (mononitroxides).

Microcrystalline samples were loaded into the sample space of a Delrin sample holder and were mounted directly to the sample rod. The sample holder was subtracted out using an empty Delrin sample holder as the background.

Poly[vinyl chloride] (9002-86-2, PVC) was precipitated from cyclohexanone/methanol and dried over P_2O_5 under vacuum to remove any trace impurities. PVC films containing 3−5% w/w biradical were placed in a clear plastic straw and mounted directly to the sample rod. As a control, **3(PhNit)₂** was tested at various concentrations. At concentrations higher than 5% w/w, biradical **3(PhNit)₂** aggregates to

form crystals that display hysteresis in the susceptibility plot. Therefore, 5% w/w was the maximum concentration used for magnetic susceptibility studies. Films were cast as solutions in methylene chloride into a glass trough and evaporated. The films were then rolled into a tight spiral for maximum sample density in the SQUID. Samples were evacuated overnight to remove any traces of solvent. A blank sample of PVC (166 mg, 6 mm length) was cast and served as the background. To obtain the best background subtraction, films were maintained at 6 mm length and ∼170 mg total mass.

X-ray Crystallography. The crystal structures of **3(PhNit)₂** (at 158 K, above the phase transition) and **4(PhNit)₂** were presented earlier.[24] Details for **1(PhNit)₂**, **2(PhNit)₂**, **6(Nit)₂**, and **7(PhNit)₂** are listed in the Supporting Information. Preliminary results for **3(PhNit)₂** at 25 K (below the phase transition) are also given in the Supporting Information, and details will be presented elsewhere.

Supporting Information Available: Crystallographic information and saturation magnetization plots (PDF and CIF). This material is available free of charge via the Internet at http://pubs.acs.org.

JA037787O

(46) Jacobs, S. J.; Shultz, D. A.; Jain, R.; Novak, J.; Dougherty, D. A. *J. Am. Chem. Soc.* **1993**, *115*, 1744−1753.

(47) Rajca, A. High-Spin Polyradicals. In *Magnetic Properties of Organic Materials*; Lahti, P., Ed.; Marcel Dekker: New York, 1999; pp 345−359.

(48) Equation 3 is related to McConnell's intermolecular exchange coupling model: McConnell, H. M. *J. Chem. Phys.* **1963**, *39*, 1910.

(49) The ratio of the average ferromagnetic *J* from Table 3 to *J* for TMM (Wenthold, P. G.; Hu, J.; Squires, R. R.; Lineberger, W. C. *J. Am. Chem. Soc.* **1996**, *118*, 475−476) ≈ 14/2625 = 0.005 ≈ $\rho_i\rho_j$ from eq 3. The *para*-carbon spin density in phenyl-*tert*-butylnitroxide is 0.06 (ref 43), so $\rho_i\rho_j$ = 0.0036, in good agreement with $\rho_i\rho_j$ from eq 3.